Exploring the mechanical performance of BaTiO3 filled HDPE nanocomposites: A comparative study of the experimental and numerical approaches

Atilla Atli, Jean-Philippe Noyel, Ahmad Hajjar, Kevin Antouly, Etienne Lemaire, Sandra Simon

Version of Record: https://www.sciencedirect.com/science/article/pii/S0032386122005511
Manuscript_bbfce79bae2b422f0eeee674fa5c2a96

Exploring the mechanical performance of $BaTiO_3$ filled HDPE nanocomposites: A comparative study of the experimental and numerical approaches

Atilla ATLI[1,*], Jean-Philippe NOYEL[1], Ahmad HaJJAR[1], Kevin Antouly[1], Etienne LEMAIRE[2], Sandra SIMON[1]

[1]Université de Lyon, ECAM LaSalle Lyon, LabECAM, F-69005, Lyon, France

[2]GREMAN, UMR-CNRS 7347, University of Tours, 16 rue Pierre et Marie Curie, BP 7155, 37071 Tours Cedex 2, France

* Corresponding author: *atilla.atli@ecam.fr*

Abstract

The mechanical behavior of $BaTiO_3$ incorporated High-Density Polyethylene (HDPE) nanocomposites up to 40% in volume is investigated experimentally through tensile tests. The results showed that Young's modulus increased with increasing amount of $BaTiO_3$ particles, indicating a higher stiffness. A numerical approach based on a micromechanical model showed the same trend, but with values lower than the experimental ones for all the composite concentrations. The influence of the particle distribution (uniform or random) in the Representative Volume Element (RVE) as well as the RVE size were particularly investigated. The effect of the strain and strain rate on the Young's modulus was highlighted experimentally and numerically. The influence of the filler particles on the strain and stress field distributions in RVE was shown to be a key parameter in the mechanical response of the nanocomposites and revealed the necessity to take into account the true behavior of HDPE in the numerical modeling.

Keywords : polymer nanocomposites, tensile test, micromechanical modelling

1 Introduction

Nowadays, high performance multifunctional materials are needed for several industrial and technological applications. The incorporation of fillers into polymer matrices is one of the most effective approaches to manufacture such materials and to develop new ones. This process has also scientific importance since the key parameters behind the modification of the polymer matrix properties by the presence of fillers are of interest.

The polymer nanocomposites, obtained by incorporation of nanoparticles in a polymer matrix are a promising family of materials since the properties of nanocomposites can be tailored for several uses by adjusting the polymer and filler parameters. Polymer nanocomposites are usually formulated by using the synergy generated by combination of both components: polymer and nanofillers. Such combination permits to use the advantages of the special characteristics of nanoparticles leading to unique properties (synergy). Prepared mixtures can also benefit from the easy processability of polymers.

The polymers used as matrix can be thermoplastics or thermosets and the fillers can be selected among metals, synthetized ceramics, minerals or natural materials depending on the limitations (economical, technical etc.) and the targeted final performance of the composite material [1].

Among the filler materials, barium titanate ($BaTiO_3$) is used for its inherent properties. Barium titanate is a ferroelectric ceramic material frequently employed by the electronics industry for various applications like capacitors, non-linear positive temperature coefficient resistors, piezoelectric transducers [2-5], high frequency applications (>GHz) in the telecommunications industry such as for beam steering, antennas and electromagnetic interference (EMI) devices [6,7]. It has also several medical applications since it is considered as biocompatible [8,9]. The incorporation of $BaTiO_3$ fillers into polymers has received special attention [10] due to the combination of excellent processability and usual properties (mechanical, thermal, electrical etc.) of each component. $BaTiO_3$ particles have been incorporated into different polymer matrices like PVDF [11], ethylene vinyl acetate (EVA) [12], polypyrrole [13], polypropylene [14], epoxy [15,16], PMMA [17], rubber [18], ethylene propylene diene monomer (EPDM) [19]. A detailed investigation has been reviewed by Su et al. [10] by targeting mainly the dielectric properties of polymer/$BaTiO_3$ composites.

Despite the fact that High Density Polyethylene (HDPE) is one of the most used thermoplastic polymers, there are a few works on the $BaTiO_3$ incorporated HDPE in the literature [20-24]. Su et al. [20] have studied the rheological, dielectric (in MHz frequency range), electrical and mechanical properties in flexural mode. They have found that the dielectric constant and flexural moduli have increased with increasing $BaTiO_3$ amount but the volume electrical resistivity has decreased. Su et al. [22] have investigated binary nano and micro sized $BaTiO_3$ particles incorporated HDPE. They have concluded that when the packing density was high, the dielectric constant, flexural, and impact strength of HDPE/$BaTiO_3$ composites simultaneously have reached the maximum value. A similar synergetic effect have also shown for PP filled by a mixture of nano sized Al_2O_3-micro sized $BaTiO_3$ particles [14]. Gonzalez-Benito et al. [23] and Martínez-Tarifa et al. [24] have prepared $BaTiO_3$/HDPE submicronic composites up to 20 wt% (*i.e.* 3.7 vol%). They have concluded that the electrical resistivity and the dielectric strength decreased with increasing $BaTiO_3$ filler amount. No detailed mechanical characterization of $BaTiO_3$-HDPE composites was found in the literature except the work of Su et al. [20] in flexural mode and, to our knowledge, no numerical investigation was realized in the past on these composites.

In the present study, the mechanical properties of $BaTiO_3$ incorporated HDPE nanocomposites are experimentally and numerically investigated. In particular, the variation of the Young's modulus of the

nanocomposites as a function of the volume fraction of the nanoparticles is assessed. The experimental evaluation is done via tensile tests on nanocomposites with filler amounts varying from 0 to 40 vol%. These tests were then completed by a numerical approach. A finite element model based on a Representative Volume Element is used to predict the mechanical behavior of the nanocomposite and to determine its Young's modulus value for various particle volume fractions. The present work highlights also the influence of different particle distributions (uniform, random) resulting different stress and strain field distributions in RVE and strongly affecting the mechanical performance of composites.

The paper is organized as follows. In Section 2, the materials used along the investigation are introduced. The preparation of the nanocomposites is described, as well as their thermal and structural characterization. Section 3 focuses on the analysis of the Young modulus of the nanocomposites. The experimental tests and results are first presented. The numerical approach is then developed and its outcomes are analyzed. A comparison between the experimental and numerical results is finally discussed and future directions of work are suggested.

2 Materials, methods, sample preparation and characterization

2.1 Materials

The polymer used in this work was HDPE provided by the manufacturer SABIC. It has a density of 0.96 g/cm^3 and a melt flow index (MFI) of 8 g/10 min (at 190°C and 2.16 kg) as indicated by the provider.

Barium titanate ($BaTiO_3$) powder purchased from Sigma Aldrich was used as filler. According to the supplier, its purity is 99.5 % and its density is 6.08 g/cm^3. The particles have a size of <2µm. In this work, the barium titanate particles were used without surface pretreatment.

2.2 Methods

The structural, thermal and mechanical properties of $BaTiO_3$ incorporated HDPE samples as well as the raw materials were characterized.

Mettler AE166 Delta range microbalance was used in simple weighing or double weighing mode for calculating the density of samples. The $BaTiO_3$ particles size and shape were characterized by Philips XL30i Scanning Electron Microscope (SEM). Elemental characterization within the SEM was assessed by Energy Dispersive X-ray spectroscopy (EDX).

For the thermal characterization, TA Q50 apparatus for Thermo Gravimetric Analysis (TGA) and TA Q20 instrument for Differential Scanning Calorimetry (DSC) were used under nitrogen flow of 90 mL/min and 50 mL/min respectively with a heating rate of 10°C/min.

In order to perform the structural characterization, Wide Angle X-Ray Diffraction (WAXD) experiments were carried out in an INEL Diffractometer by using a Cobalt source (λ=1.789 Å, 25 KV, 25 mA). X-Rays were detected by a 120° hemispherical multichannel detector.

A Perkin Elmer Spectrum Two model of Attenuated Total Reflection-Fourier Transformed Infrared Spectroscopy (ATR-FTIR) was used to determine the absorption bands of the samples. The FTIR spectra were obtained with a resolution of 4 cm^{-1}.

As for the mechanical characterization, the tensile tests were performed by employing a Shimadzu AGS-X test machine equipped by a video extensometer, and later compared to numerical simulations.

2.3 Sample preparation

The blends of $BaTiO_3$ and HDPE were prepared using a twin screw Brabender blender. First, HDPE pellets were melted at 170°C-180°C in the blender bowl having a volume of 35 cm^3. Barium titanate powder was then gradually added in the molten HDPE up to a desired final composition. The torque generated by the twin screw with adjustable rotating speed was recorded as a function of time during blending and the screws were kept at a constant torque during approximately 10 min once the torque was stabilized. Barium titanate-HDPE blends with four different volume compositions were prepared: 10 vol%, 20 vol%, 30 vol% and 40 vol%. Three batches were prepared for each composition in order to have enough material to produce a dozen of samples. After blending, the obtained pads were grinded and injected by using an ARBOURG All Rounder 270S injection mold with an 18 mm diameter screw. The typical temperatures during injection molding were set between 160°C and 200°C, depending on the barium titanate filler amount *i.e.* the higher the barium titanate amount the higher the injection temperature. Neat HDPE samples were also injected as reference for comparison. The mixtures with filler amount higher than 40 vol% were very difficult to blend and to inject in our preparation conditions. The highest filler amount used in this work was then 40 % in volume. The injection flow was fixed to 45 cm^3/sec with a pressure of 1800 bars. The injection mold was kept at room temperature. The tensile test samples having different composition (filler amount from 0 to 40 vol%) are shown in Fig. 1.

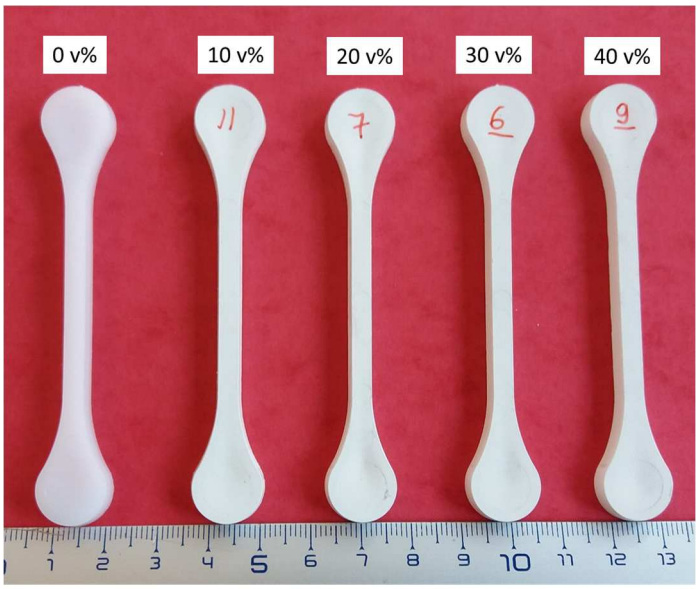

Fig. 1. Injected tensile test composite samples with different amount of $BaTiO_3$ incorporated in HDPE matrix: from left to right: 0 vol% (neat HDPE), 10 vol% $BaTiO_3$, 20 vol% $BaTiO_3$, 30 vol% $BaTiO_3$, 40 vol% $BaTiO_3$.

One of the important parameters in the case of filled polymer composites is the filler particle size. In order to determine the $BaTiO_3$ particle size distribution, the images of powder particles were taken by SEM as shown in the inset of Fig. 2. The dimension of $BaTiO_3$ particles was measured over around 120 particles and the distribution was plotted (Fig. 2). On this figure, the histogram represents the experimental particle size distribution and the dotted line is the Gaussian distribution plotted from the experimental measurements. The particle distribution has a maximum around a particle size span of 0.4-0.5 µm and the particle size lies below 2 µm as specified by the $BaTiO_3$ powder supplier.

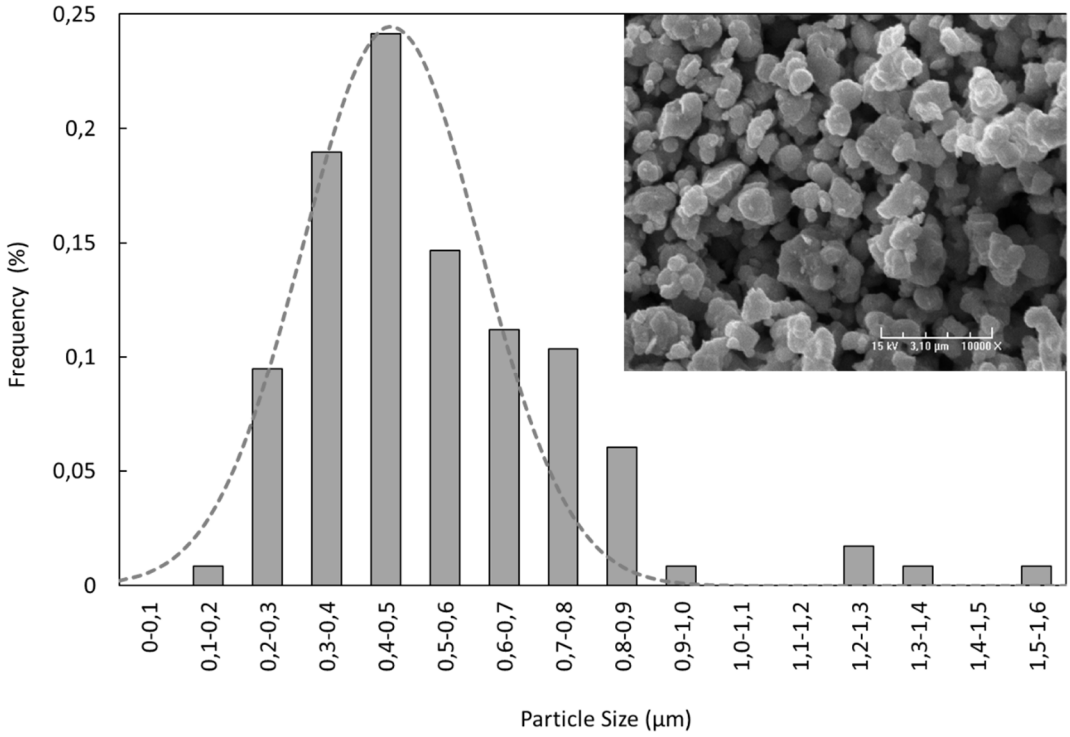

Fig. 2. Particle size distribution of the commercial $BaTiO_3$ powder used as filler and SEM image of the powder (in the inset)

2.4 Density of HDPE-$BaTiO_3$ composites

The experimental density of composite samples was calculated by employing the double weighing method in air and then in water at room temperature. The density of composites was then calculated by using the following expression:

$$d = \frac{m_{air}}{m_{air} - m_w} d_w \qquad (1)$$

where d and d_w are the densities of composite samples and water (d_w was taken 1 g/cm^3) respectively and m_{air} and m_w are the measured masses in air and in water respectively. For each composite composition, at least three samples were weighed and the mean value was calculated.

The density of neat HDPE and that of pure $BaTiO_3$ were taken 0.96 g/cm^3 and 6.08 g/cm^3 respectively as given by suppliers for the theoretical density calculation taking into account the amount of HDPE and $BaTiO_3$ incorporated. The density of neat HDPE given by the polymer supplier was also experimentally verified. The experimental and theoretical densities are shown in Table 1.

Amount of Barium Titanate (vol%)	Theoretical Density (g/cm^3)	Experimental mean density (g/cm^3)	Relative Difference (%)
0	0,96	0,96	-
10	1,47	1,44±0.04	2,22
20	1,98	1,96±0.02	1,22
30	2,49	2,45±0.01	1,88
40	3,01	2,95±0.01	1,97

Table 1: Theoretical and experimental densities of neat and $BaTiO_3$ incorporated HDPE samples

The nanocomposite densities increase with increasing $BaTiO_3$ filler amount. The experimental and theoretical densities are very close, as the relative difference between theoretical and experimental

densities remains below a few percent. This observation would indicate that the composite samples have a homogenous composition and exclude the excessive amount of porosity.

2.5 Thermal Characterization: Thermo Gravimetric Analysis (TGA) and Differential Scanning Calorimetry (DSC) analysis

The TGA and DSC experiments were performed on $BaTiO_3$ filled HDPE composites as well as on neat HDPE with a heating rate of 10°C/min under nitrogen atmosphere.

For neat HDPE, at the end of the experiment almost no residue was detected in TGA (Fig. 3a). For all other composites, the weight of the residue at the end of the experiments corresponded nearly to the theoretical $BaTiO_3$ filler amount. It was also observed that the onset of the polymer decomposition temperature shifted to the higher values with increasing amount of $BaTiO_3$ filler suggesting that the thermal degradation of composites was retarded by the presence of $BaTiO_3$ nanoparticles.

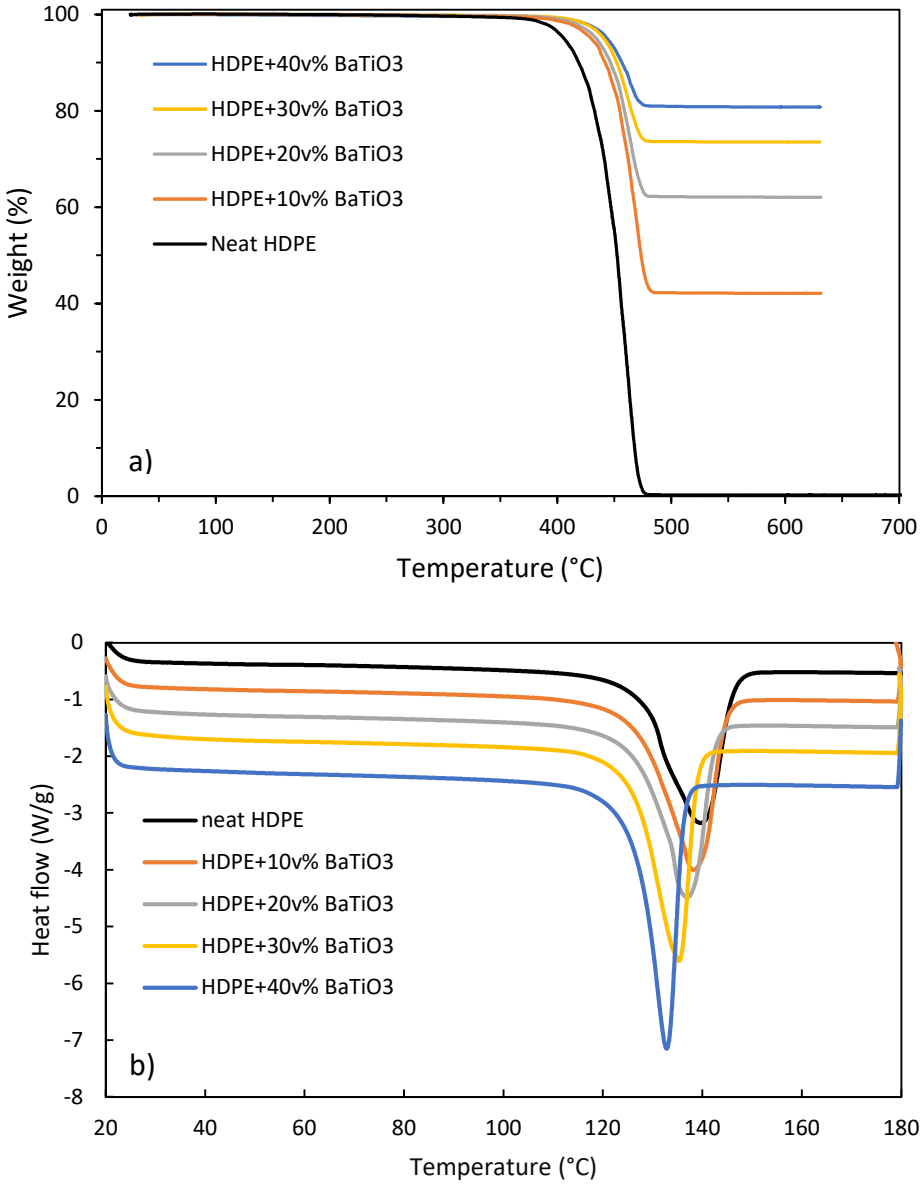

Fig. 3. TGA a) and DSC thermograms b) of $BaTiO_3$-HDPE nanocomposites

Gonzales-Benito et al. have found a similar trend [23]. They have prepared the composites of HDPE filled by submicronic $BaTiO_3$ particles (mean diameter 200 nm) by using high-energy ball milling

technique. They have studied HDPE filled $BaTiO_3$ up to 20wt% by TGA and found that the thermostability of nanocomposites has been improved by increasing the $BaTiO_3$ content since the onset of the thermodegradation process has slightly increased and the temperature of the maximum thermal degradation rate has not been modified by the presence of barium titanate particles. Nevertheless in their work, the maximum $BaTiO_3$ filler amount was 20 % in weight corresponding to approximately 3.7 % in volume and was far below our smallest amount of composite *i.e.* 10 vol%.

The DSC thermograms were recorded for the series of $BaTiO_3$ filled HDPE nanocomposites (Fig. 3b). The thermal program was as following: after the stabilization of sample temperature at 20°C, the samples were heated up to 180°C with a heating rate of 10°C/min under nitrogen atmosphere. The heat flow was normalized to the amount of polymer.

During heating from 20°C to 180°C, only the melting peaks of HDPE were observed. It was remarked that the maximum of the melting peak temperature (T_{mm}) shifted to the lower temperatures in the presence of $BaTiO_3$ nanoparticles: from 139.7°C in neat HDPE to 132.8°C in 40 vol% $BaTiO_3$. This observation would indicate that the incorporation of $BaTiO_3$ nanoparticles modified the thermal properties HDPE matrix.

It is known that the degree of crystallinity of a polymer affects its mechanical properties. It is then important to characterize the microstructure of the samples. DSC is one of the common methods for determining the degree of crystallinity of polymers. The degree of crystallinity (X_c) is often determined by measuring the amount of heat required to melt a given polymer (melting enthalpy, ΔH_m) compared to the heat required to melt the same polymer having a crystallinity of 100% (melting enthalpy of fully crystalline polymer, $\Delta H_m^{100\%}$) as written in equation (2)

$$X_c(\%) = \frac{\Delta H_m}{\Delta H_m^{100\%}} 100 \qquad (2)$$

The enthalpy of fusion of composites is estimated from the DSC thermograms. For the composite samples, only the HDPE undergoes the melting process in the studied temperature range. The melting peaks observed on DSC thermograms correspond only to HDPE and the mass of $BaTiO_3$ filler particles was subtracted from the total mass in order to normalize the measured heat to the amount of HDPE. The melting enthalpy of samples was calculated by using Universal Analysis software from the area of the melting peaks shown in Fig. 3b by taking into account the baseline. $\Delta H_m^{100\%}$ was taken 293 J/g as the melting enthalpy of 100% crystalline HDPE [25].

The variation of relative crystallinity of HDPE with $BaTiO_3$ filler amount was shown in Fig. 4. The degree of crystallinity of the samples was found around 70% and seemed to be unaffected by the presence of $BaTiO_3$ particles.

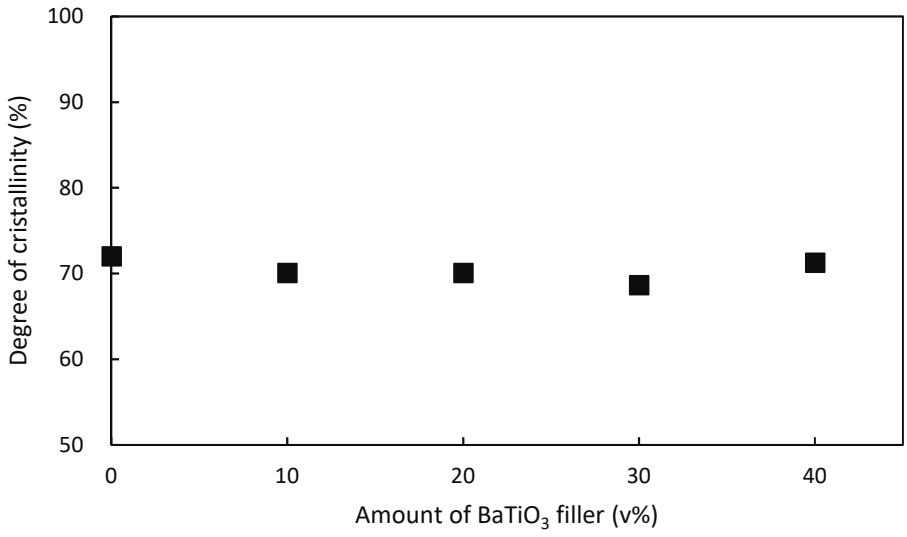

Fig. 4. Variation of HDPE crystallinity with different amount of incorporated $BaTiO_3$ in HDPE

Su et al. [21,22] have found a similar trend on HDPE/$BaTiO_3$ composites: a decrease in melting peak temperatures and the degree of crystallinity of the $BaTiO_3$ incorporated HDPE composites compared to virgin HDPE. They have found a decrease of degree of crystallinity from 66.9% for pure HDPE to 54.9% and 47.2% for 30 vol% and 40 vol% $BaTiO_3$ filled HDPE, respectively [21]. However, in their work the surface of $BaTiO_3$ particles was modified by a coupling agent, which can restrict the motion of polymer chains to form a crystalline structure. Gonzales-Benito et al. [23] have also found a relative crystallinity of around 50% for neat HDPE and HDPE filled up to 20 wt% (around 3.7 vol%) by $BaTiO_3$ particles. Our results are then consistent with those found in the literature [21-23].

2.6 Structural characterization

2.6.1 SEM observations on the fracture surfaces

In order to observe the particle distribution on composite samples, SEM observation were performed on the facture surfaces of $BaTiO_3$ filled polymers nanocomposites. To avoid the charge-up effect, the fracture surfaces of specimens were initially coated with a thin layer of gold using a Polaron E5000 sputter-coating unit (Polaron Ltd., London, UK) prior to SEM observations. Subsequently, the SEM scans were taken on the facture surface of $BaTiO_3$-HDPE nanocomposites (Fig. 5).

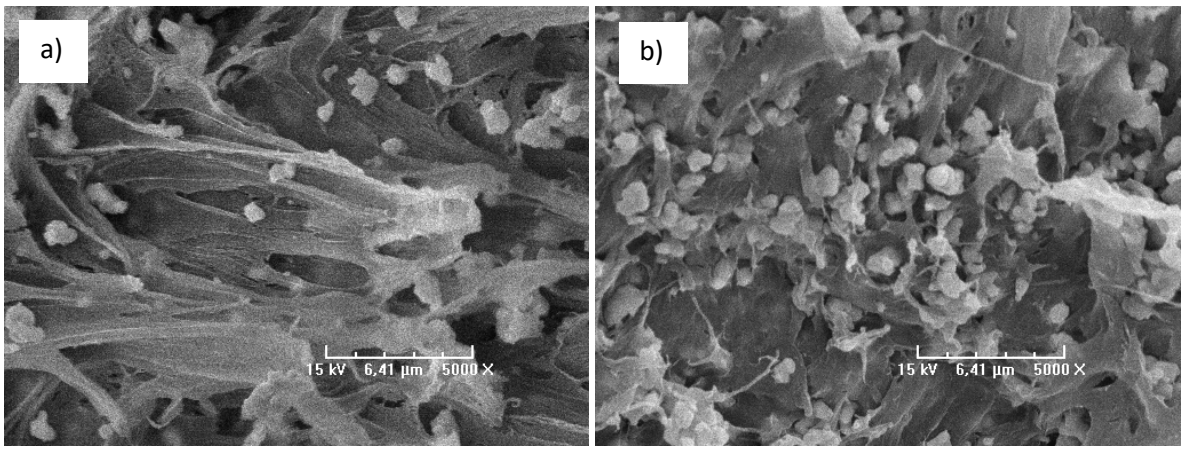

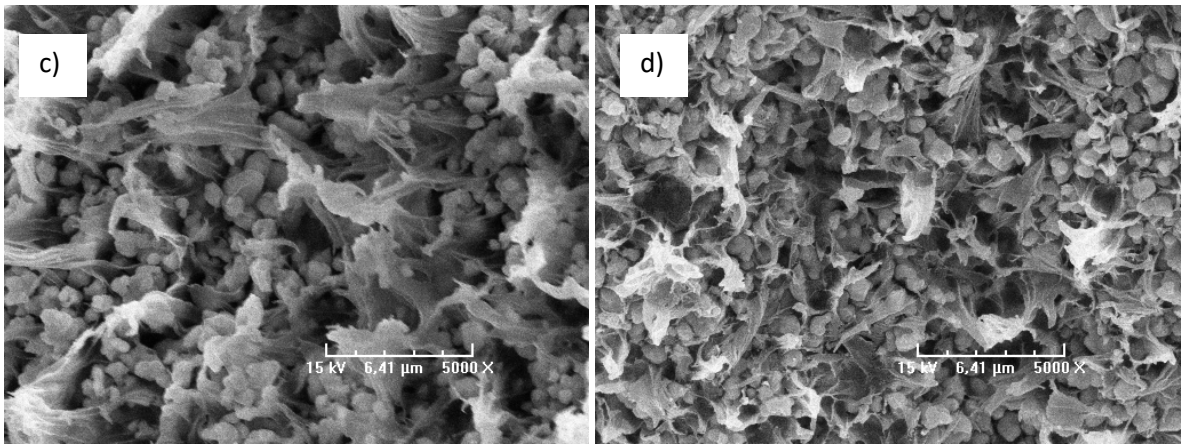

Fig. 5. SEM images on fracture surfaces of 10v% a), 20v% b), 30v% c), 40v% d) $BaTiO_3$ filled HDPE nanocomposites

As seen on the SEM images on Fig. 5, the individual $BaTiO_3$ nanoparticles were easily distinguished. The particles were randomly distributed without any big cluster formation. In fact, the aggregation of nanofillers can influence the mechanical properties of polymer nanocomposites [26].

2.6.2 FTIR and WAXD analysis

The FTIR spectra were performed on HDPE-$BaTiO_3$ composite samples as well as on neat HDPE used as reference. The samples characterized in this experiment were those obtained after injection without any heat treatment.

The FTIR spectra were displayed on Fig. 6a. The neat HDPE spectrum demonstrated typical bands at 2914 cm^{-1} and 2848 cm^{-1} that were attributed to asymmetric and symmetric stretching vibrations of C–H group, respectively [27]. A band around 1470 cm^{-1} originated from C-H bending of CH_2 groups. Moreover, the presence of a typical band at 718 cm^{-1}-728 cm^{-1} represents CH_2 rocking mode in CH_2 groups.

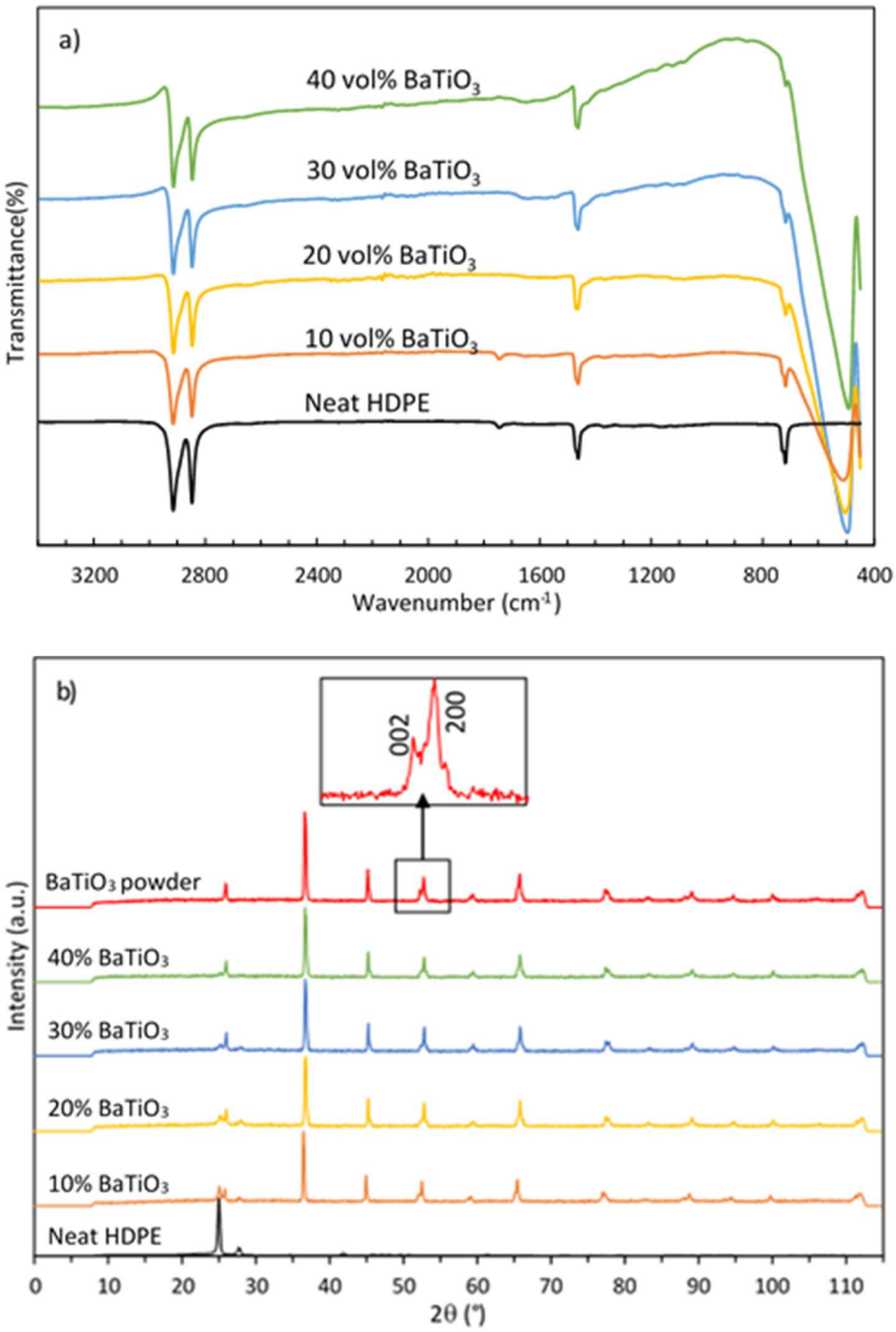

Fig. 6. FTIR spectra a) and WAXD diffractograms b) on neat and $BaTiO_3$ filled HDPE nanocomposites

The WAXD diffraction experiments were performed on injected samples (Fig. 6b). The diffractogram on neat HDPE showed a strong peak at 25° and two others at 27.8° and 41.9° corresponding to the (110), (200) and (020) crystalline planes of HDPE [28]. The WAXD patterns obtained on $BaTiO_3$ powder exhibited several sharp diffraction patterns indicating a high crystallinity structure. $BaTiO_3$ exists in four allotropic structures: orthorhombic, rhombohedral, tetragonal and cubic [29]. The existence of one or another allotrope of $BaTiO_3$ depends on several parameters (temperature, powder preparation technique, the size of the precipitated crystals etc.) [29,30]. The splitting of (200) pattern at around 50-55° in cubic lattice into (200) and (002) in tetragonal lattice is a fingerprint of tetragonal structure [31,32]. In our case, we remarked two patterns at around 52-53° corresponding to the (200) and (002)

diffraction planes (inset in Fig. 6b), indicating a tetragonal crystal structure of $BaTiO_3$ particles used as filler.

For 10 vol% and 20 vol% filled HDPE samples, we observed both HDPE and $BaTiO_3$ patterns indicating that filler particles were successively incorporated into polymer matrix. The $BaTiO_3$ patterns become dominant and HDPE patterns disappear gradually with increasing filler amount.

3 Results

The mechanical properties of $BaTiO_3$ filled HDPE as well as neat HDPE were characterized in tensile tests. A Finite Element (FE) approach by using ANSYS was also employed to model the mechanical behavior in order to better understand HDPE/$BaTiO_3$ composite system.

3.1 Experimental Approach

3.1.1 Tensile test experiments

Tensile test experiments were carried out on injected samples shown in Fig. 1. A first series of tensile test experiments was performed with a crosshead speed of 1 mm/min (Fig. 7). On neat polymer, the maximum stress was around 18 MPa for strains below 0.2. The maximum stress in the 0-0.2 strain region increased for 20 vol% and 30 vol% of $BaTiO_3$ and then considerably decreased to around 15 MPa for 40 vol% $BaTiO_3$ filled HDPE. Conversely, the strain at break decreased with increasing filler amount indicating the brittle nature of the filled HDPE compared to the neat HDPE.

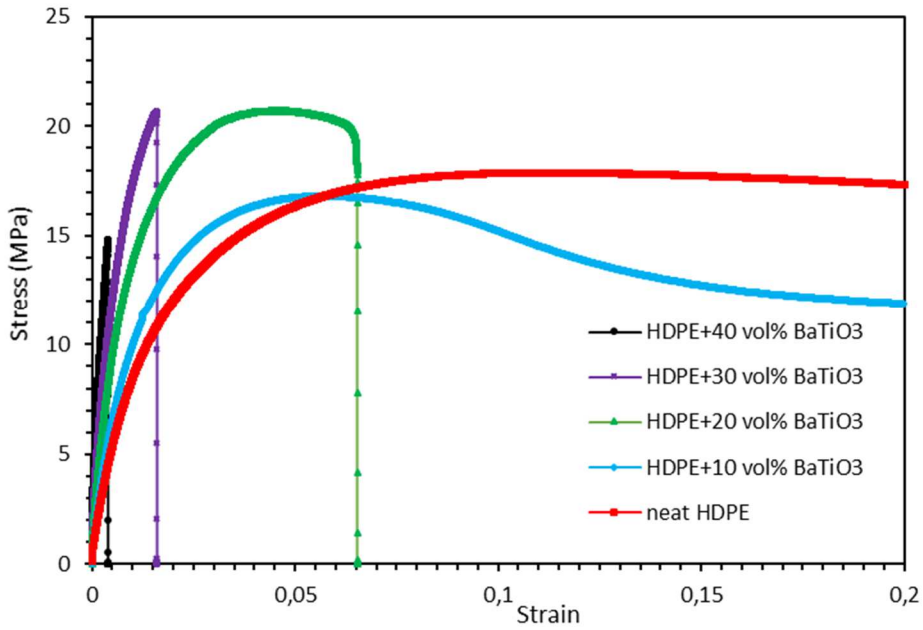

Fig. 7. Tensile test experiments on neat and BaTiO3 filled HDPE

3.1.2 Tensile test: focus on Young's modulus

In order to determine the Young's modulus, a set of tensile tests was carried out on the specimens with a crosshead speed of 1 mm/min (Fig. 8). Maximum tensile force was limited to 100 N (around 5.5 MPa), far below the yield strength in order to repeat the tests on the same sample.

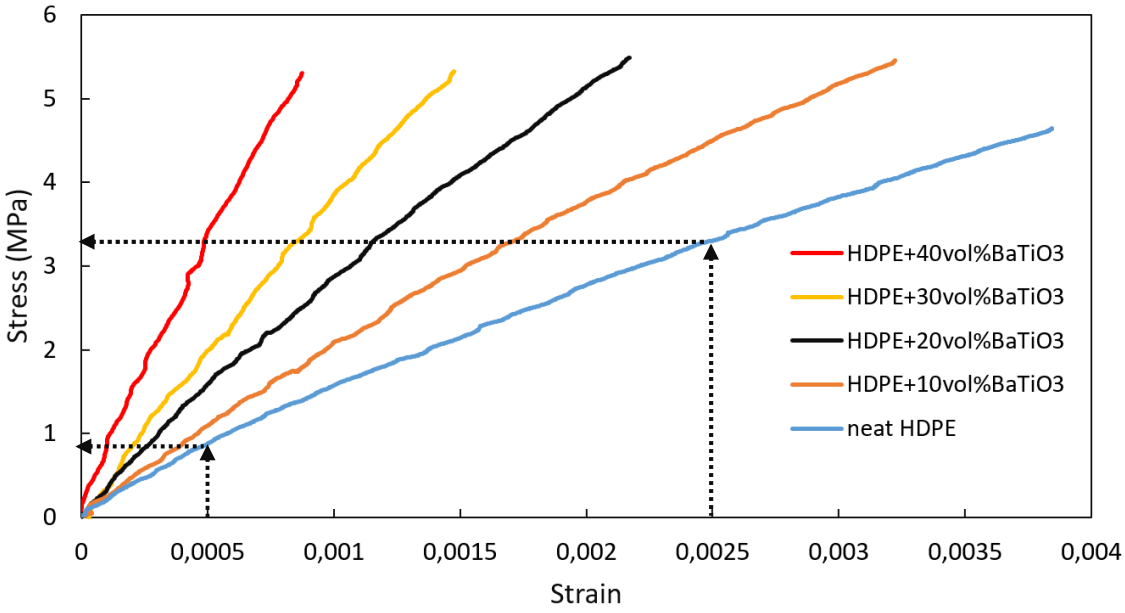

Fig. 8. The stress-strain curves on neat and $BaTiO_3$ filled HDPE composites with different filler amount

The Young's Modulus of neat HDPE samples were estimated by using ISO 527-1 Standard by calculating the slope of the straight line between 0.0005 and 0.0025 strain points on stress-strain curves (dotted lines with arrows on Fig. 8). Otherwise, for nanocomposites, due to the impossibility to use the same strain range to evaluate Young's moduli, the stresses corresponding to 0.0005 and 0.0025 strain points were used.

The variation of Young's moduli with $BaTiO_3$ filler amount was plotted (Fig. 9). The dotted line was drawn for guiding eye. At least four tests were done for a given composition.

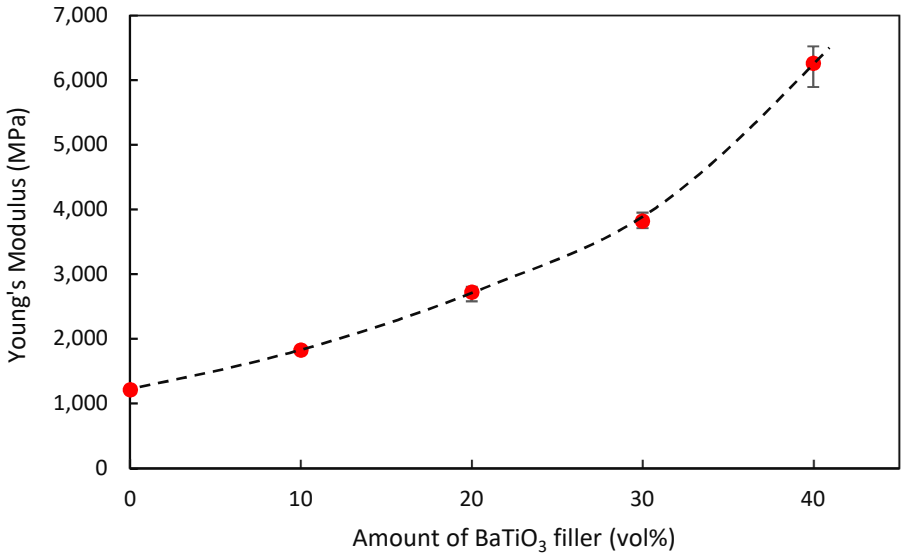

Fig. 9. The variation of Young's modulus of HDPE-$BaTiO_3$ nanocomposites with $BaTiO_3$ filler amount

On neat HDPE, Young's modulus was calculated around 1200 MPa. In the literature, several values of Young's modulus for HDPE were found depending on the parameters (temperature, strain rate, sample crystallinity and dimensions, sample processing, etc.) [33-35]. Kalay et al. [33] have determined a Young's modulus of 1402 MPa on HDPE samples prepared by conventional molding. Amjadi et al. [34] have calculated 800 MPa with a crosshead speed of 1 mm/min in tensile test at room temperature for

a virgin HDPE sample with a thickness of 4 mm prepared by injection molding. Elleuch et al. [36] have determined Young's modulus between 978 MPa to 1523 MPa for the strain rates of $4x10^{-3}$ to $4x10^{-1}$ s^{-1} respectively. It is then important to take some precautions when the literature values are mentioned and compared to our experimental results.

As seen on Fig. 9, Young's modulus increased with increasing $BaTiO_3$ amount in HDPE indicating a strengthening process.

3.2 Numerical approach

The mechanical properties of polymer nanocomposites have been predicted for example by analytical and numerical methods for polymer nanocomposites [37-43]. In this work, we used a numerical approach by using Finite Element analysis.

3.2.1 Description of the model

In order to investigate the mechanical behavior of $BaTiO_3$ filled HDPE nanocomposites, 3D Finite Element Analysis (FEA) was performed using the Material Designer application and mechanical application in the commercial software ANSYS (ANSYS 2020 R1).

For a starting point, a basic model including a spherical $BaTiO_3$ particle centered in a cubic polymer matrix was considered as a Representative Volume Element (RVE) (Fig. 10a). In this model called "Simple Cubic (SC)", the diameter of the spherical $BaTiO_3$ particles (d_p) is set to 0.5 µm as measured by SEM (Fig. 2). The edge length a of the cube was adjusted in a way that the desired amount of particle filler fraction in polymer matrix was obtained. Such a RVE has commonly exploited because of its simplicity and its high symmetry reducing then the computation time [41,44]. Four other particle distributions were also investigated as shown on Fig. 10: Body Centered Cubic (BCC) (Fig. 10b), Face Centered Cubic (FCC) (Fig. 10c), random particle distribution in 3D space with a constant particle diameter d_p=0.5 µm (Fig. 10d), random particle distribution in 3D space with a normal particle size distribution (mean particle diameter d_{mean}=0.5 µm and standard deviation (SD)=0.15 µm) (Fig. 10e).

The contact between nanoparticles and polymer matrix with an interface/interphase control the efficiency of the stress transfer through polymer to nanofillers [45] and play an important role on the mechanical behavior. The models used in the analytical approaches are frequently adjusted to obtain a good correlation with the experimental results [37].

In this work using a numerical approach, a perfect bonding contact type between HDPE and $BaTiO_3$ particles was applied. In fact, among the contact types, only the perfect bonding permits to increase the Young's modulus with the incorporation of filler particles [46].

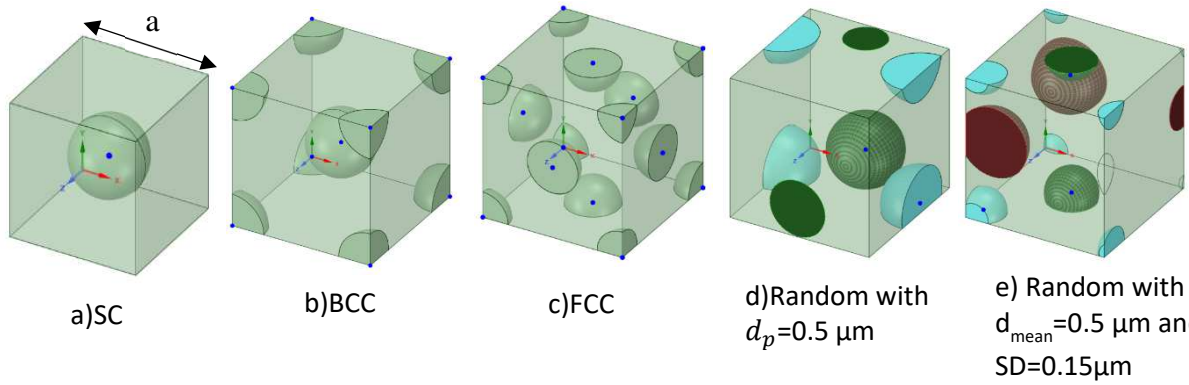

Fig. 10. Studied Representative Volume Elements (RVE)

In order to compute the Young's modulus of the nanocomposites, the RVE were subjected to a tensile load case by imposing a displacement in x direction (δ_x). Two cases with two types of boundary conditions were applied as illustrated in Fig. 11. In the first case (Fig. 11a), all faces of RVE were fixed

immobile except that the face at $x = a$ was permitted to move uniformly in x direction. The reaction forces F_x, F_y and F_z in x,y and z directions were calculated. In the second case (Fig. 11b), the displacement δ_y at face $y = a$ and δ_z at face $z = a$ were free to move uniformly at a constant value and the reaction force F_x was calculated.

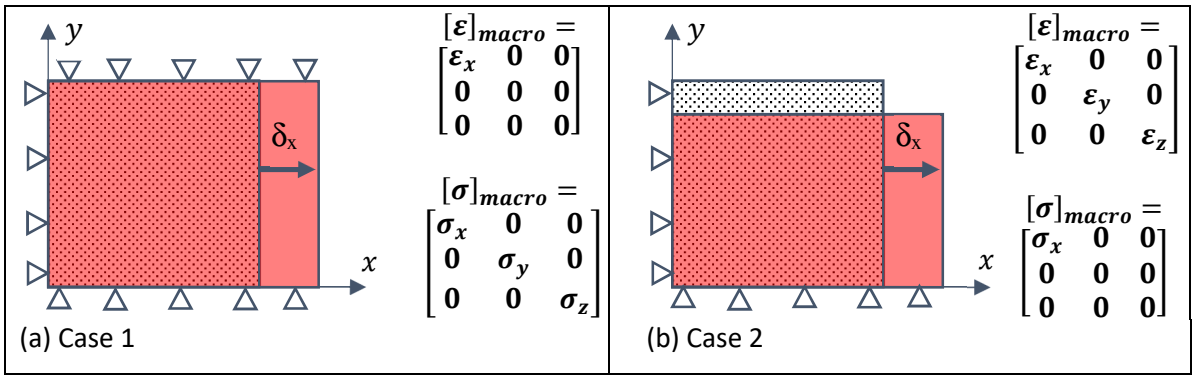

Fig. 11. Two different boundary conditions used in our calculation Case 1 a) and Case 2 b)

The macroscopic strain is defined in equation (3), and the macroscopic stress is computed with the reaction force considering equation (4). Then the equivalent Young's modulus of the RVE is computed using these values; for example, for case 2, the Young's modulus is given in equation (5).

$$\varepsilon_x = {}^{\delta_x}/_{a} \qquad (3)$$

$$\sigma_x = {}^{F_x}/_{a^2} \qquad (4)$$

$$E = {}^{\sigma_x}/_{\varepsilon_x} \qquad (5)$$

These two cases are very similar and for a given composite composition, Young's modulus computed with both cases was identical. In fact, Case 1 corresponds to the boundary conditions used in Material Designer, and Case 2 was introduced to analyze stress and strain distribution in the RVE, because it is an uniaxial load case, which corresponds to the experimental tensile test.

3.2.2 Influence of $BaTiO_3$ Young's Modulus

The mechanical behavior of particles and matrix are supposed to be elastic isotropic linear. Concerning the matrix and particle engineering data (Young's modulus and Poisson's ratio), the Young's modulus of $BaTiO_3$ particles was unknown. For bulk $BaTiO_3$, several values of Young's modulus can be found in the literature. Den Toonder et al. [47] have measured a macroscopic average elastic constant of 146.1 GPa and calculated 162.8 GPa in plane strain and 145.1 GPa in plane stress for tetragonal $BaTiO_3$. The elastic moduli of 120-183 GPa have been reviewed by Bowen et al. [48] and an elastic modulus of around 120 GPa has been found by Cheng et al. at room temperature [2]. The Young's moduli of 139.59 GPa and 154.16 GPa have been measured in two different domains of tetragonal $BaTiO_3$ single crystal [49]. An elastic modulus of $BaTiO_3$ up to 167.9 GPa has been measured depending on the used precursor for $BaTiO_3$ processing [50].

Nevertheless, these bulk Young's modulus values depend on several parameters (sintering conditions, electrical condition: poled-unpoled, crystal structure (cubic, tetragonal, etc), temperature, etc.). It was then difficult to select a Young's modulus value of $BaTiO_3$ among the values found in the literature for FE calculations. Especially, the Young's modulus was given for a bulk $BaTiO_3$ material that can diverge while $BaTiO_3$ is in powder form. For this reason, we first determined the influence of Young's modulus of $BaTiO_3$ particles on the Young's modulus of the RVE in a simple cubic distribution. Young's modulus of $BaTiO_3$ was varied from 80 GPa to 300 GPa by fixing its Poisson's ratio to 0.3, and the Young's modulus and Poisson's ratio of neat HDPE to 1206 MPa (as found by using the tensile tests in the

previous experimental section) and 0.42 respectively. Evolution of the Young's moduli of composites as a function of Young's modulus of $BaTiO_3$ particles was plotted for four compositions of nanocomposites (Fig. 12). The Young's modulus of neat HDPE calculated from tensile test experiments was also shown as dotted line on this figure for comparison.

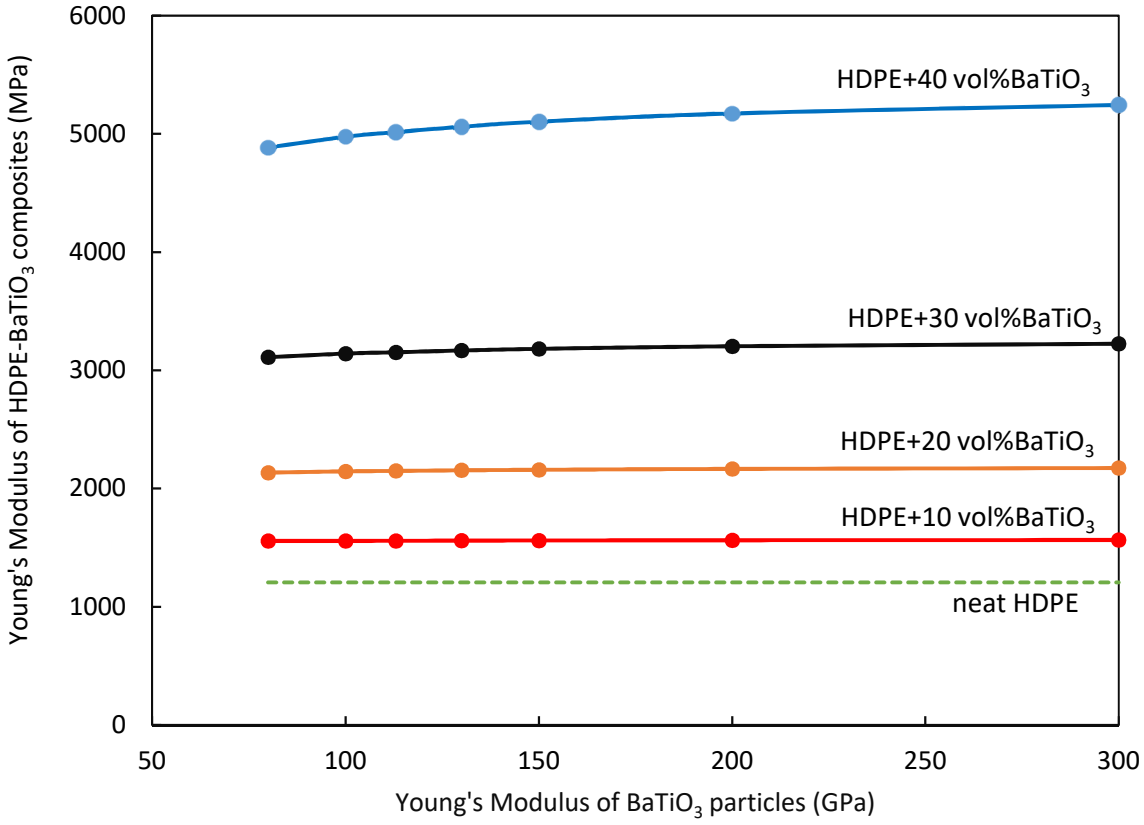

Fig. 12. Evolution of Young's modulus for different composition of HDPE-$BaTiO_3$ nanocomposites with Young's modulus of $BaTiO_3$ particles

For a given filler fraction, Young's modulus of HDPE-$BaTiO_3$ nanocomposites seems to be constant and independent of the Young's modulus of $BaTiO_3$ particles in the range of 80 GPa-300 GPa. This range includes the experimental values mentioned previously. When Young's modulus of filler is very high compared to that of polymer matrix, beyond a certain ratio of filler and matrix Young's moduli, Young's Modulus of composites were not affected by further increase of the Young's modulus of filler particles. A similar trend has already been observed for thermal conductivity studies of filled polymers by using FE analysis [51]. We then decided to use a Young's modulus of 200 GPa for $BaTiO_3$ particles for the rest of the analysis. This chosen value is not far from the bulk $BaTiO_3$ Young's modulus and permits to use a unique set of particle and matrix properties for FE calculations of all HDPE-$BaTiO_3$ composites.
The engineering data of each material are then summarized in Table 2.

	Young's Modulus (MPa)	Poisson's ratio
$BaTiO_3$ particles	200 000	0.30
HDPE polymer matrix	1 206	0.42

Table 2: Engineering constants of used materials

3.2.3 Outcomes from numerical calculations

The Young's Modulus for different composite compositions was computed by using five models and represented in Fig. 13. As seen on Fig. 13, the Young's Modulus of composites increases with increasing $BaTiO_3$ amount.

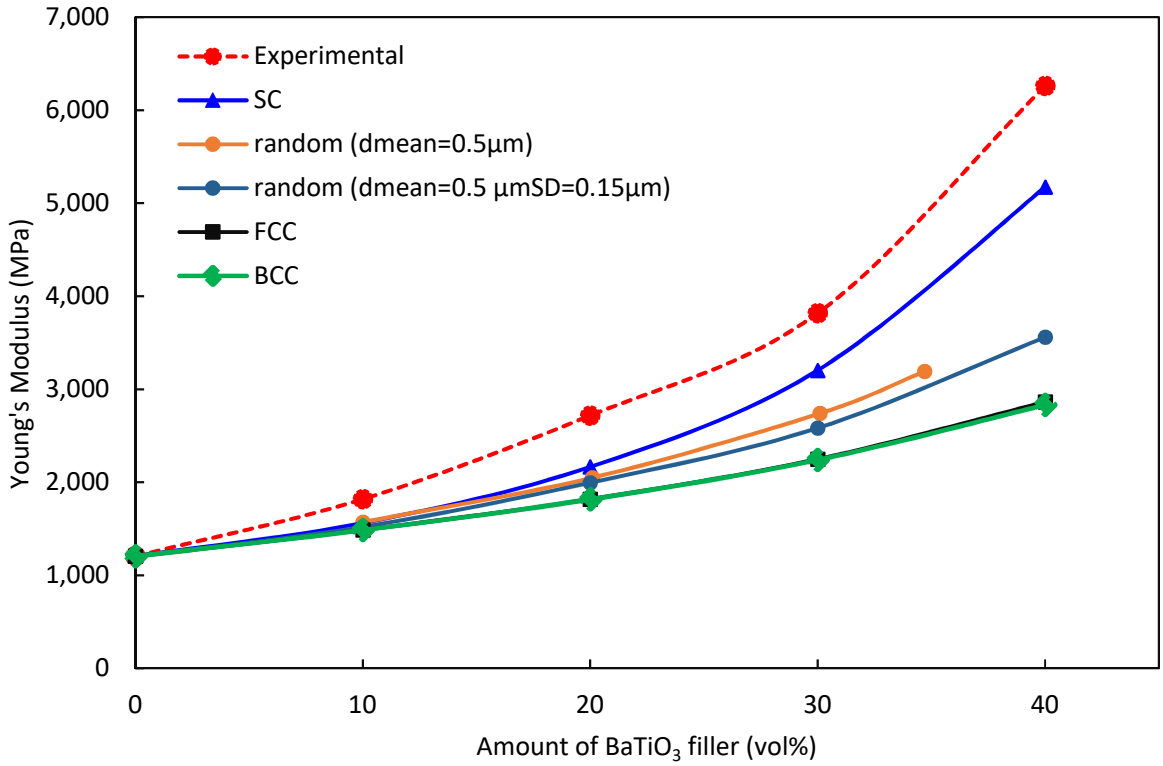

Fig. 13. Computed Young's modulus as a function of $BaTiO_3$ filler amount. The experimental results are also added for comparison

For a given $BaTiO_3$ fraction, the experimental Young's Moduli were higher than all the calculated ones. Computational approach highlighted the strong influence of particle distribution on estimated Young's modulus. The results obtained by using FCC and BCC configurations were very close and gave the smallest Young's moduli among the used models (Fig. 13). The SC particle distribution gave the highest Young's moduli calculated by FE analysis. The SC model yielded also the closest values to the experimental results. The random distribution with a constant particle diameter of 0.5 µm and a normal distribution of particle size (mean particle diameter and standard deviation were 0.5 µm and 0.15 µm respectively) led to the intermediate Young's moduli between SC and FCC-BCC models (Fig. 13). However, the experimental values were found higher than the values obtained from all the theoretical models considered here. Balać et al. [41] have found the same trend for elastic properties of particulate polymer composite by using FE method, *i.e.* higher Young's modulus values in SC particle distribution than in FCC distribution.

3.2.3.1 Influence of particle distribution

In previous section, the particle distribution demonstrated to have a strong influence of the RVE on Young's modulus (Fig. 13). For such a RVE, the limits for Young's modulus value are given by Voigt's Model (upper bound) and Reuss Model (lower bound). Voigt's model considers a constant strain in the RVE (Particle and matrix are in parallel) and Reuss Model considers a constant stress (Particle and matrix are in serial).

In order to understand the influence of particle distribution on the equivalent Young's modulus, the SC, BCC and FCC uniform particle distributions were investigated with Case2 boundary conditions (Fig. 11b). The imposed displacement δ_x was adjusted in a way that the resultant macroscopic stress becomes 1 MPa.

The stress field distribution in each RVE was shown in Fig. 14. On this figure, the first column (Fig. 14a, d and g) concerns the RVE in SC, BCC and FCC particle distribution, respectively. The second column (Fig. 14b, e and h) illustrates the stress field distribution within the SC, BCC and FCC, respectively. The third column (Fig. 14c, f and i) shows the stress distribution on a cross section in the mid-plane of RVE (obtained from second column), in SC, BCC and FCC respectively.

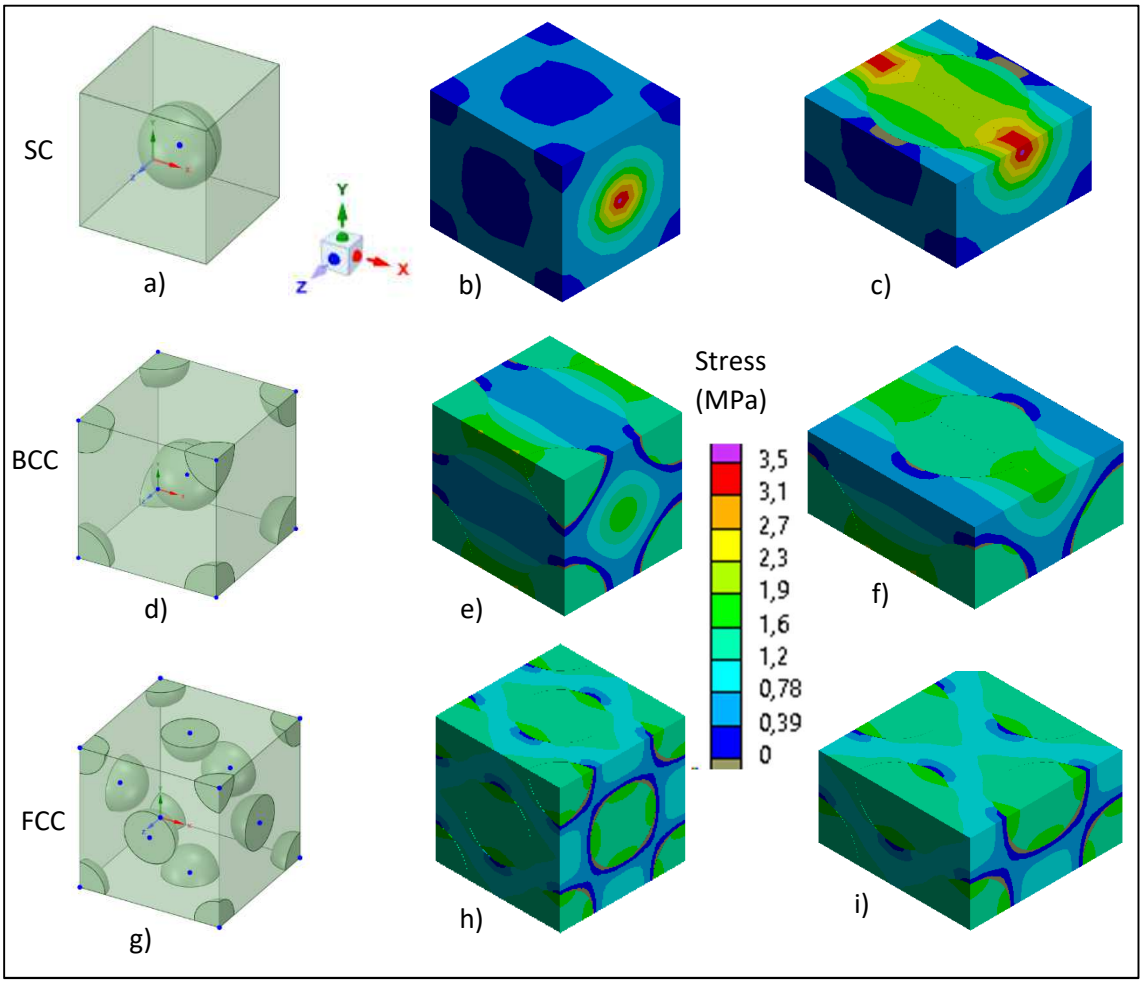

Fig. 14. Three uniform SC, BCC and FCC distribution of $BaTiO_3$ particles in HDPE matrix when a stress of 1 MPA was applied in x direction

The stress distribution is very similar in BCC and FCC particle distributions and more uniform than for the SC distribution. So the BCC and FCC distributions are represented better by Reuss model, which explains a lower value for the equivalent Young's Modulus.

To complete this analysis, we could observe that the stress seems to be travelling through a plane formed by polymer and particles. The RVE could then be schematically represented in Fig. 15, which corresponds to a combination of Reuss model and Voigt's model. In this representation a channel is formed only by HDPE (channel 1 in Fig. 15) and a second channel is composed by both HDPE and $BaTiO_3$ filler particles (channel 2 in Fig. 15). In SC distribution, the size of channel 1 is more important, and so the behavior is closest to the Voigt's model.

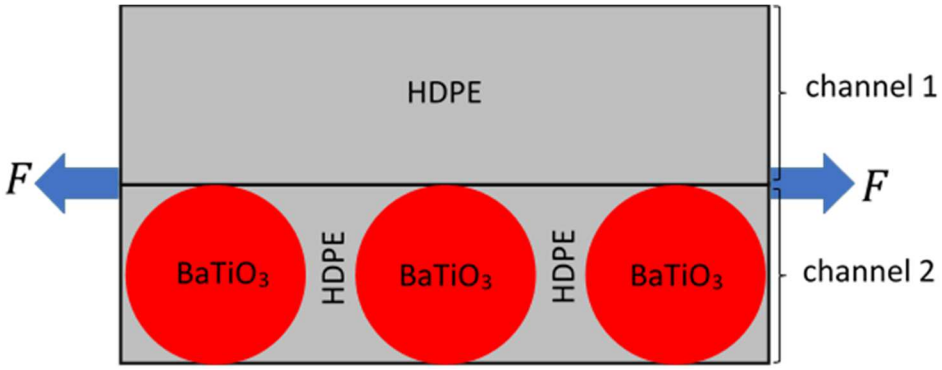

Fig. 15. Mechanical representation of HDPE-$BaTiO_3$ nanocomposites as a channel structure for uniform particle distribution

3.2.3.2 Influence of the RVE size

For random particles distribution, Young's Modulus depends on the size of the RVE. This size is defined by the parameter λ by using equation (6) where λ is a number bigger than 1:

$$a = \lambda \times d_p \qquad (6)$$

Only the results computed with the model having a constant particle diameter are presented in this section. For each composition, the influence of the size of RVE was investigated by modeling ten different random distributions for each size *i.e.* $\lambda = 2$, $\lambda = 3$, $\lambda = 4$, etc. The Young's modulus is computed in the three directions (x, y and z) for each simulation. The equivalent E was calculated from the mean value of three components (E_x, E_y and E_z). Two examples are given in Table 3 for $\lambda = 2$ and $\lambda = 6$ for a filler amount of approximately 30 vol%.

λ	Filler amount (vol%)	Young's Modulus (MPa)	Average Young's Modulus (MPa)	Standard deviation (MPa)	Standard deviation (%)
2	32.7	E_x	3266	259	8%
		E_y	3364	203	6%
		E_z	3443	299	9%
		E_{mean}	3358	210	6,2%
6	30.1	E_x	2747	36	1,3%
		E_y	2732	32	1,2%
		E_z	2743	32	1,2%
		E_{mean}	2741	26	1,0%

Table 3: Value of Young's Modulus for λ=2 and λ=6 for approximately 30 vol% filler amount. Mean Young's Moduli are calculated over 10 random distributions

It should be noted that the real filler amount depends on the size of the RVE: for example, with $\lambda = 2$, when a filler amount of 30% is required, the exact filler amount obtained is 32.7%. Moreover, the maximum filler amount obtained in our work does not exceed to approximately 35 vol% since the particles cannot allowed to touch each other. All the results were summarized in Fig. 16.

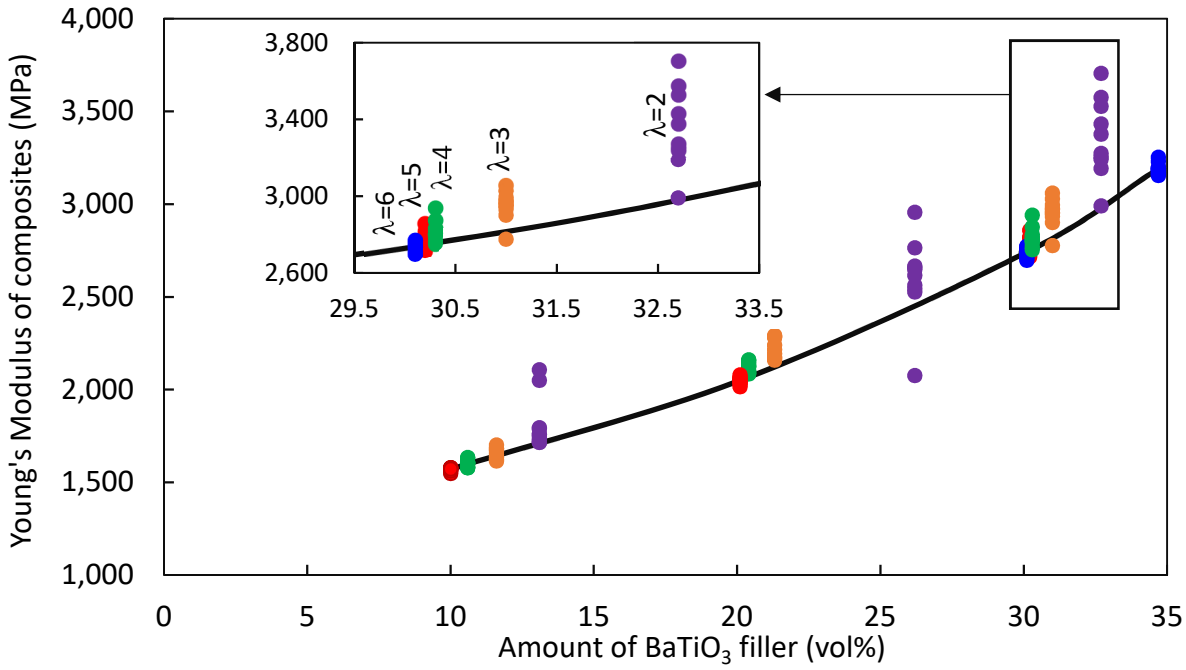

Fig. 16. Young's modulus obtained with random particle distribution with a constant particle diameter of 0.5µm

With increasing value of λ parameter, the standard deviation between calculated Young's moduli decreased. When the value of the standard deviation becomes smaller than 1%, the size of the RVE was considered as sufficient and the mean Young's Modulus (of ten random distribution for a given composition) is considered as the real value of the RVE (black curve in Fig. 16). In the inset of this figure, the convergence of the Young's modulus for five different λ values was also shown for a composition of approximately 30 vol%. Moreover, the macroscopic behavior tends to become isotropic for higher λ values: Young's moduli were nearly the same in the three directions (Table 3).

3.2.3.3 Analysis of the stress and strain fields in composites and influence of strain rate

In this section, the distribution of stress and strain in HPDE was further studied by employing the random distribution with particles having a constant diameter of d_p=0.5 µm.

The imposed displacement in x direction δ_x was chosen, as the resultant macroscopic strain of 0.001=0.1%. An example of local strain (Fig. 17a) and local stress (Fig. 17b) distributions both in x direction in only HDPE part of composite was given in Fig. 17 for 30 vol% of filler showing a heterogeneous strain and stress distribution in HDPE.

For this example, the value of the macroscopic stress is 2.711 MPa and the mean stress only on polymer part of composite is 1.967 MPa *i.e.* lower than the macroscopic one.

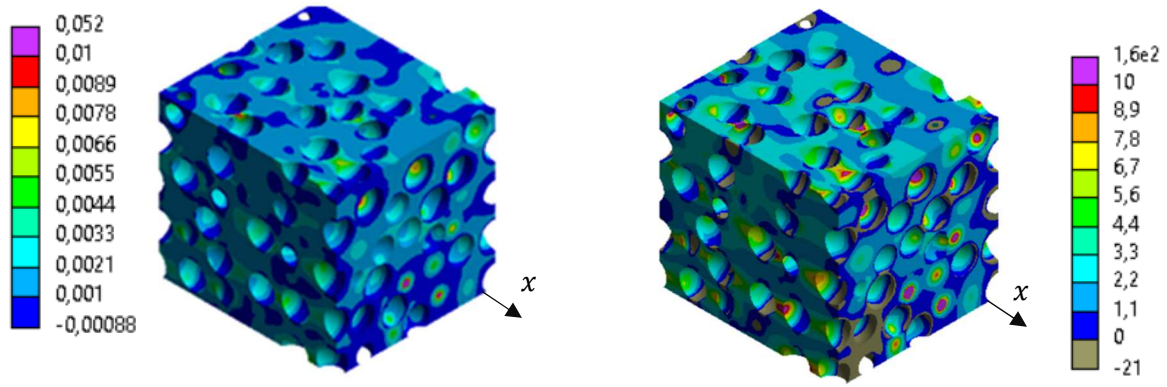

(a) local strain in x direction only in HDPE (b) local stress (MPa) in x direction only in HDPE

Fig. 17. Strain a) and stress b) distribution for a filler amount of 30% and a macroscopic strain of 0.1% in x direction (the $BaTiO_3$ particles are hidden for a better visibility of stress and strain in HDPE matrix)

The resulting macroscopic stress and strain in RVE as well as the mean stress and strain only in polymer part with different filler amount are summarized in Table 4.

	Amount of $BaTiO_3$ filler (vol%)			
	10	20	30	34.7
Macroscopic ε_x in RVE (%)	0.100	0.100	0.100	0.100
Mean ε_x in only HPDE part (%)	0.111	0.126	0.143	0.154
Macroscopic σ_x in RVE (MPa)	1.569	2.027	2.711	3.165
Mean σ_x in only HPDE part (MPa)	1.393	1.681	1.967	2.155

Table 4: Macroscopic stress and strain in RVE and average stress and strain in only in polymer part in nanocomposites with four different compositions

For a given filler amount, the mean strain in only HDPE part of composite is higher than the macroscopic strain imposed on the RVE. A direct effect of this observation is that the effective strain rate on the HDPE is much higher than the strain rate imposed on the RVE. Moreover, it is well known that the strain rate has a great influence on the behavior of HDPE.

The tensile tests presented in Fig. 8 were carried out with a crosshead speed of 1mm/min. In order to characterize the influence of strain rate, other experimental tensile tests on neat HDPE were carried out with a crosshead speed varied from 0.1 mm/min to 5 mm/min. Experimental stress-strain curves are presented on Fig. 18a. The effect of the strain rate appears clearly on these curves: the slope of the stress-strain curve increases with increasing crosshead speed.

It is worth noting that for a given crosshead speed, the stress-strain curve cannot be considered as linear, and the slope *i.e.* Young's modulus varies also with strain. In order to characterize the slope of these curves in Fig. 18a, the tangent Young's moduli were estimated for each strain taking a crosshead speed. The results are presented in Fig. 18b. The evolution of these tangent Young's moduli confirms the dependency on both the strain and the strain rate.

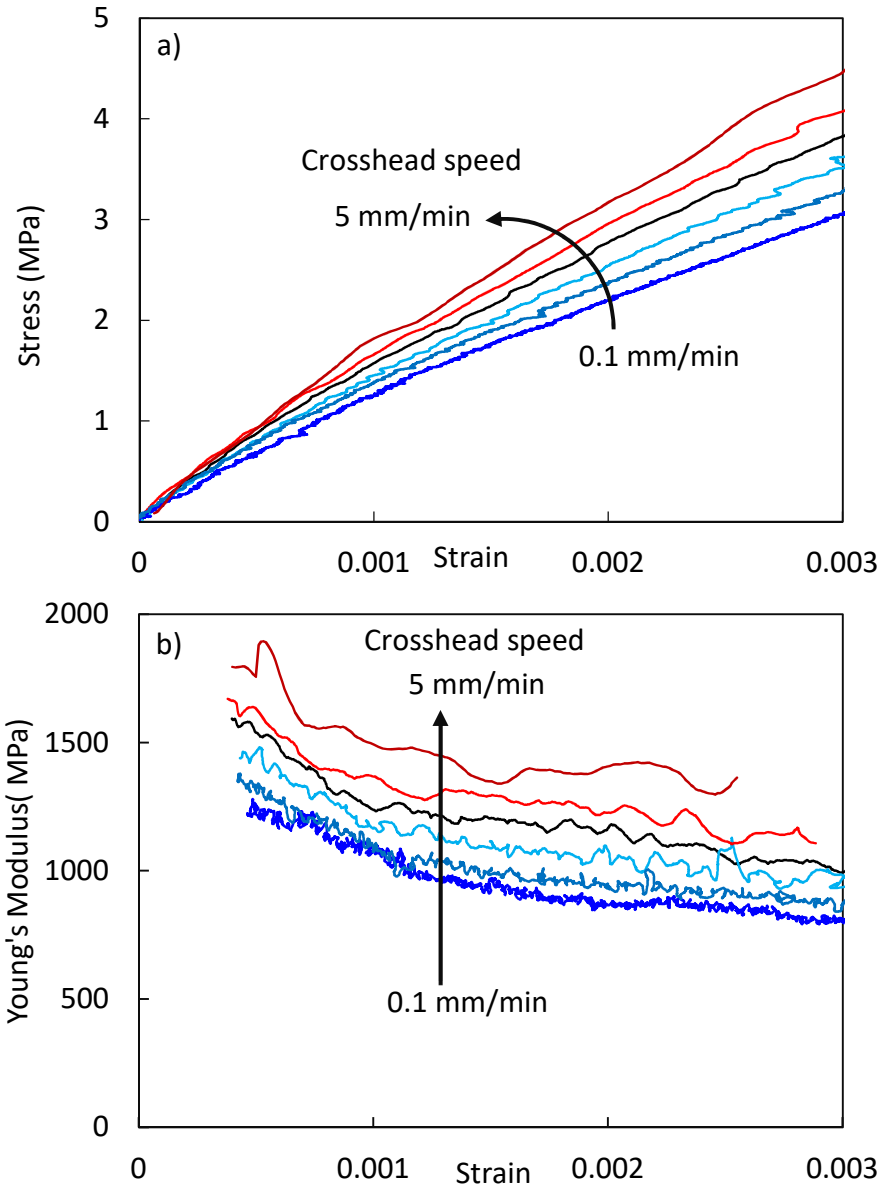

Fig. 18. Stress-strain curves of neat HDPE for different crosshead speeds (from 0.1 mm/min to 5 mm/min) in tensile test experiments.

Considering (*i*) the large heterogeneity of strain distribution in HDPE and (*ii*) the dependence of Young's modulus to strain and strain rate, the assumption of a linear elastic behavior could seem too restrictive.

4 Discussion and Conclusions

Nanocomposites of HDPE-$BaTiO_3$ were prepared with a volume proportion of 10 %, 20 %, 30 % and 40 % and shaped in an injection mold. The density of injected nanocomposite samples was measured and fitted well with the theoretical density values excluding important amount of voids in samples. The structural properties of samples were characterized by FTIR, WAXD and SEM. FTIR spectra did not reveal a significant modification of HDPE polymer matrix by the presence of $BaTiO_3$. WAXD indicated the $BaTiO_3$ filler particles were in tetragonal crystal structure and successfully incorporated into polymer matrix. The SEM observations on fractured surfaces showed a random particle distribution and without the formation of big $BaTiO_3$ particle clusters. The thermal properties of HDPE polymer matrix were modified by the presence of $BaTiO_3$ fillers. The onset of degradation temperature was

shifted to the higher values with increasing filler amount compared to neat HDPE as analyzed by TGA. The DSC results indicated that the melting temperature was decreased with increasing amount of $BaTiO_3$ fillers in HDPE. The degree of crystallinity of all the samples was around 70-75% as revealed by DSC. The presence of $BaTiO_3$ fillers seemed no significant influence on the degree of crystallinity. This conclusion is in line with the FTIR analysis where no remarkable modifications were detected in polymer FTIR bands when particles are incorporated.

The Young's modulus of nanocomposites determined from the experimental tensile tests increased with increasing filler amount. In order to further analyze the mechanical behavior of nanocomposites, Finite Element analysis in tensile mode were performed with several approaches. The influence of random and uniform (SC, BCC and FCC) particle distributions in polymer matrix was studied. The contact between the spherical $BaTiO_3$ particles and polymer matrix was considered as "perfect bonded" permitting to increase the stiffness of composites by incorporation of filler particles in HDPE.

The experimental Young's moduli obtained from tensile tests showed a variation trend similar to the one obtained using FE analysis, but the experimental values were always higher than the numerical ones. (Fig. 13). Moreover, the simple cubic uniform distribution results are the closest FE results compared to the experimental ones. However, uniform particle distribution is not a realistic model for the HDPE-$BaTiO_3$ nanocomposites. In fact, the random distribution models are more realistic and represent better the nanocomposites since the filler particles are randomly distributed in the tested specimens as verified by SEM on fracture surfaces. The difference between experimental and simulation results can be due to the several reasons. We can mention:

- The filler particles are considered spherical in FE analysis. In reality, the particles are not perfectly spherical (inset in Fig. 2). The shape of particles can play a role in the FE simulation of mechanical behavior.
- There can be a percolation effect [52] of $BaTiO_3$ particles in HDPE matrix, which was not taken into account in the FE models. In fact, the percolation can modify the mechanical behavior of nanocomposites [53].
- In some cases of polymer nanocomposites, an interphase model (onion model) has been proposed [38,42,43,54]. In this model, it was considered that the polymer properties surrounding the filler particles have been modified. The perturbed region around the particles was represented as several thin layers with a known thickness and the polymer properties are assumed to be gradually modified from the surface of the particle within a distance in the interphase region. Since the interphase thickness and the number of layers were unknown in our case, this model was not applied. Especially for a random particle distribution, interphase should be manually designed around each particle.
- In the numerical model, the polymer matrix was assumed to exhibit a linear elastic behavior *i.e.* a constant Young's Modulus. However, it was shown that when a stress is applied onto HDPE based composite samples, their mechanical response depends on the strain and strain rate as discussed. A viscoelastic constitutive model for the polymer in which the stress varies with both the strain and strain rate seems to be more suitable for implementation in the numerical simulations aiming to reproduce the experimental findings.

Overall, an improved model with the real filler particle shape (other than the spherical), including the interphase around particles as well as the polymer viscoelastic behavior would permit to fit the experimental and the FEM results and can be the subject of future investigations. The outcomes of this work can be extended to other particulate filled polymers composites by modifying the engineering parameters of filler and polymer components

Acknowledgement

We thank Mr. Abhishek THIGALE from National Institute of Technology Karnataka (India) for his internship during which he participated in this research project.

References

[1] R. N. Rothon, Ed., Particulate-Filled Polymer Composites, Rapra Technology Limited, 2003.

[2] B.L. Cheng, M. Gabbay,G. Fantozzi, W. Duffy Jr., "Mechanical loss and elastic modulus associated with phase transitions of barium titanate ceramics" *J. Alloys Compd.* 211/212 (1994)352-355.

[3] V. Buscaglia, M. T. Buscaglia and G. Canu, "$BaTiO_3$-Based Ceramics: Fundamentals, Properties and Applications" in *Encyclopedia of Materials: Technical Ceramics and Glasses*, vol. 3, M. Pomeroy, Ed., Elsevier, 2021, pp. 311-344.

[4] S. B. Baştürk, C. E. J. Dancer, T. McNally, "Dielectric performance of composites of $BaTiO_3$ and polymers for capacitor applications under microwave frequency" *J. Appl. Polym. Sci.* 138(22) (2021)50521.

[5] H. Yang, W. Bao, Z. Lu, L. Li, H. Ji, Y. Huang, F. Xu, G. Wang, D. Wang, "High-energy storage performance in $BaTiO_3$-based lead-free multilayer ceramic capacitors" *J. Mater. Res.* 36(2021) 1285-1294.

[6] P. Saini, M. Arora, G. Gupta, B.K. Gupta, V.N. Singh, V. Choudhary, "High permittivity polyaniline-barium titanate nanocomposites with excellent electromagnetic interference shielding response" *Nanoscale,* 5(10)(2013)4330-4336.

[7] S. B. Baştürk, C. E. J. Dancer, T. Mcnally, "Fabrication and characterization of composites of a perovskite and polymers with high dielectric permittivity" *Mater. Res. Bull.* 135(2021)111126.

[8] J. Ball, B. A Mound, J. C. Nino, J. Allen, "Biocompatible evaluation of barium titanate foamed ceramic structures for orthopedic applications" *J. Biomed. Mater. Res. Part A,* 102(7)(2014) 2089-2095.

[9] C. Shuai, G. Liu, Y. Yang, W. Yang, C. He, G. Wang, Z. Liu, F. Qi, S. Peng, "Functionalized $BaTiO_3$ enhances piezoelectric effect towards cell response of bone scaffold" *Colloids Surf. B* 185(2020) 110587.

[10] J. Su, J. Zhang, "Recent development on modification of synthesized barium titanate($BaTiO_3$) and polymer/$BaTiO_3$ dielectric composites" *J. Mater. Sci.: Mater Electron,* 30(2019)1957-1975.

[11] L. Xie, X. Huang, K. Yang, S. Li and P. Jiang, "“Grafting to” route to PVDF-HFP-GMA/$BaTiO_3$ nanocomposites with high dielectric constant and high thermal conductivity for energy storage and thermal management applications" *J. Mater. Chem. A,* 2(2014)5244.

[12] M. Chikhi, B. Agoudjil, M. Haddadi and A. Boudenne, "Numerical modelling of the effective thermal conductivity of heterogeneous materials" *J. Thermoplast. Compos. Mater.* 26(2013) 336.

[13] K. Ahmed, F. Kanwal, S. M. Ramay, S. Atiq, R. Rehman, S. M. Ali and N. S. Alzayed, "Synthesis and Characterization of $BaTiO_3$/Polypyrrole Composites with Exceptional Dielectric Behaviour" *Polymers,* 10(2018)1273.

[14] J. Yao, L. Hu, M. Zhou, F. You, X. Jiang, L. Gao, Q. Wang, Z. Sun and J. Wang, "Synergistic Enhancement of Thermal Conductivity and Dielectric Properties in Al_2O_3/$BaTiO_3$/PP Composites" *Materials* 11(2018)1536.

[15] W. Yang, S. Yu, S. Luo, R. Sun, W-H Liao, C-P Wong, "A systematic study on electrical properties of the BaTiO3–epoxy composite with different sized $BaTiO_3$ as fillers" *J. Alloys and Compd.* 620 (215)315-323.

[16] L. Ramajo, M. Reboredo, M. Castro, "Dielectric response and relaxation phenomena in composites of epoxy resin with $BaTiO_3$ particles" *Composites: Part A,* 36(2005)1267-1274.

[17] R.K. Goyal, S.S. Katkade, D.M. Mule, "Dielectric, mechanical and thermal properties of polymer/$BaTiO_3$ composites for embedded capacitor" *Composites: Part B,* 44(2013)128-132.

[18] A. Kumar, D. Ahmad, K. Patra and M. Hossain, "Enhancement of electromechanical properties of natural rubber by adding barium titanate filler: An electro-mechanical study" *J. Appl. Polym. Sci. 138(39)(2021)*50991.

[19] J. Su, J. Zhang, "Improvement of electrical properties and thermal conductivity of ethylene propylene diene monomer (EPDM)/barium titanate ($BaTiO_3$) by carbon blacks and carbon fibers" *J Mater Sci.: Mater Electron.* 28(2017)5250-5261.

[20] J. Su, J. Zhang, "Comparison of rheological, mechanical, electrical properties of HDPE filled with $BaTiO_3$ with different polar surface tension" *Appl. Surf. Sci. Part A,* 388(2016)531-538.

[21] J. Su, J. Zhang, "Preparation and properties of Barium titanate ($BaTiO_3$) reinforced high density polyethylene (HDPE) composites for electronic application" *J. Mater. Sci.: Mater Electron.* 27(2016)4344-4350.

[22] J. Su, J. Zhang, "Effect of Arrangement of Nano and Micro Barium Titanate ($BaTiO_3$) Particles on the Enhanced Dielectric Constant of High-Density Polyethylene (HDPE)/$BaTiO_3$" *J. Polym. Sci., Part B: Polym. Phys.* 56(2018)1101-1108.

[23] J. Gonzalez-Benito, J. Martinez-Tarifa, M.E. Sepúlveda-García, R.A. Portillo, G. Gonzalez-Gaitano, "Composites based on HDPE filled with $BaTiO_3$ submicrometric particles. Morphology, structure and dielectric properties" *Polym. Test.* 32(2013)1342-1349.

[24] J. M. Martínez-Tarifa, M.E. Sepúlveda-García, R. Portillo-Romaní, J. González-Benito, "Uniformly Dispersed Submicrometric $BaTiO_3$ Particles in HDPE Based Composites, Morphology, structure and dielectric properties" in *IEEE International Conference on Solid Dielectrics (ICSD)*, June 30-July 4 (2013), Bologna, Italy.

[25] J. Morawiec, A. Pawlak, M. Slouf, A. Galeski, E. Piorkowska, N. Krasnikowa, "Preparation and properties of compatibilized LDPE/organo-modified montmorillonite nanocomposites" *European Polym. J.* 41(2005)1115-1122.

[26] X. Ma, Y. Zare and K. Y. Rhee, "A Two-Step Methodology to Study the Influence of Aggregation/Agglomeration of Nanoparticles on Young's Modulus of Polymer Nanocomposites" *Nanoscale Res. Lett.* 12(2017)621.

[27] A. K. Sahu, K. Sudhakar, R.M. Sarviya, "Influence of U.V light on the thermal properties of HDPE/Carbon black composites" *Case Stud. Therm. Eng.* 15(2019)100534.

[28] M. E. Mahmoud, M. A.Khalifa, R. M.El-Sharkawy, M. R.Youssef, "Effects of Al_2O_3 and BaO nano-additives on mechanical characteristics of high-density polyethylene" *Mater. Chem. Phys.* 262(2021)124251.

[29] D. Nicheva, R. Harizanova, V. Ilcheva, I. Mihailova, T. Petkova, P. Petkov, "$BaTiO_3$ Structure as a Function of the Preparation Method" in *Nanoscience and Nanotechnology in Security and Protection against CBRN Threats*, M. E. A. C. P. Plamen Petkov, Ed., Dordrecht, Springer (2020) 76.

[30] S. Hao, D. Fu, J. Li, W. Wang, B. Shen, "Preparation and Characterization of Ag-Doped $BaTiO_3$ Conductive Powders" *International Journal of Inorganic Chemistry (*2011) article ID 837091.

[31] A.A. Thanki, R.K. Goya, "Study on effect of cubic- and tetragonal phased $BaTiO_3$ on the electrical and thermal properties of polymeric nanocomposites" *Mater. Chem. Phys.* 183(2016)447-456.

[32] H. Ding, L. Lin, D. Gu, S. Shang, "Synthesis and surface modification of submicron $BaTiO_3$ powders via a facile surfactant-assisted method" *Ceram. Int.* 46(2020)22040-22048.

[33] G. Kalay, R.A. Sausa, R.L. Reis, A.M. Cunha, M.J. Bevis, "The enhancement of the mechanical properties of High-Density Polyethylene" *J. Appl. Polym. Sci.* 73(1999)2473-2483.

[34] M. Amjadi, A. Fatemi, "Tensile Behavior of High-Density Polyethylene Including the Effects of Processing Technique,Thickness, Temperature, and Strain Rate" *Polymers* 12(2020)1857.

[35] S.M. Zebarjad, S.A. Sajjadi, "On the strain rate sensitivity of HDPE/$CaCO_3$ nanocomposites" *Mat. Sci. Eng. A* 475(2008)365-367.

[36] R. Elleuch and W. Taktak, "Viscoelastic Behavior of HDPE Polymer using Tensile and Compressive Loading" *J. Mater. Eng. Perform.* 15(1)(2006)111-116.

[37] Y. Zare, K. Y. Rhee, S-J. Park, "Predictions of micromechanics models for interfacial/interphase parameters in polymer/metal nanocomposites" *Int. J. Adhes. Adhes.* 79(2017)111-116.

[38] Y. Zare, "Modeling approach for tensile strength of interphase layers in polymer nanocomposites" *J. Colloid Interface Sci.* 471(2016)89-93.

[39] Y. Zare, "Study on interfacial properties in polymer blend ternary nanocomposites: Role of nanofiller content" *Comput. Mater. Sci.* 111(2016)334-338, 2016.

[40] Y. Zare, K. Y. Rhee, "Development of Hashin-Shtrikman model to determine the roles and properties of interphases in clay/$CaCO_3$/PP ternary nanocomposite" *Appl. Clay Sci.* 137(2017) 176-182.

[41] I. Balac´, M. Milovancevic´, C. Tang, P. S. Uskokovic, D. P. Uskokovic, "Estimation of elastic properties of a particulate polymer composite using a face-centered cubic FE model" *Mater. Lett.* 58(2004)2437-2441.

[42] S. Boutaleb, F. Zaïri, A. Mesbah, M. Naït-Abdelaziz, J.M. Gloaguen, T. Boukharouba, J.M. Lefebvre, "Micromechanical modelling of the yield stress of polymer-particulate nanocomposites with an inhomogeneous interphase" *Procedia Eng.* 1(2009)217-220.

[43] S. Boutaleb, F. Zaïri, A. Mesbah, M. Naït-Abdelaziz, J.M. Gloaguen, T. Boukharouba, J.M. Lefebvre, "Micromechanics-based modelling of stiffness and yield stress for silica/polymer nanocomposites" *Int. J. Solids Struct.* 46(2009)1716-1726.

[44] C.P. Tsui, C.Y. Tang, T.C. Lee, "Finite Element Analysis of polymer composites filled by interphase coated particles" *J. Mater. Process. Technol.* 117(2001)105-110.

[45] W. Peng, S. Rhim, Y. Zare, K. Y. Rhee, "Effect of "Z" Factor for Strength of Interphase Layers on the Tensile Strength of Polymer Nanocomposites" *Polym. Compos.* 40(3)(2019)1117-1122.

[46] A. Atli, J-Ph. Noyel, S. Simon, "Comparaison des propriétés des polymères nanocomposites de Polyéthylène haute densité(PEHD)-Al_2O_3 obtenues par approche théorique et expérimentale" in *22ème Congrès Français de Mécanique (2015)* Lyon, France.

[47] M. J. den Toonder, J. A. W. van Dommelen and F. P. T. Baaijens, "The relation between single crystal elasticity and the effective elastic behaviour of polycrystalline materials: theory,measurement and computation" *Modelling Simul. Mater. Sci. Eng.* 7(1999)909-928.

[48] C. R. Bowen, A. C. Dent, R. Stevens, M. G. Cain, A. Avent, "A new method to determine the un-poled elastic properties of ferroelectric materials" *Sci. Technol. Adv. Mater.* 18(1)(2017)264-272.

[49] Y-B. Park, M. J. Dicken, Z-H. Xu, X. Li, "Nanoindentation of the a and c domains in a tetragonal $BaTiO_3$ single crystal" *J. Appl. Phys.* 102(2007)1, no. 083507.

[50] S-S. Ryu, H-T. Kim, H-J. Kim, S. Kim, "Characteriation of mechanical properties of $BaTiO_3$ ceramic with different types of sintering aid by nanoindentation" *J. Ceram. Soc. Japan,* 117(7)(2009)811-814.

[51] D. Kumlutas, I. H. Tavman, "A Numerical and Experimental Study on Thermal Conductivity of Particle Filled Polymer Composites" *J. Thermoplast. Compos. Mater.* 18(4)(2006)441-455.

[52] J. C. Martinez-Garcia, A. Serraïma-Ferrer, A. Lopeandía-Fernández, M. Lattuada, J. Sapkota, J. Rodríguez-Viejo, "A Generalized Approach for Evaluating the Mechanical Properties of Polymer Nanocomposites Reinforced with Spherical Fillers" *Nanomaterials* 11(4)(2021)830.

[53] Y. Zare, K. Y. Rhee, "A multistep methodology for calculation of the tensile modulus in polymer/carbon nanotube nanocomposites above the percolation threshold based on the modified rule of mixtures" *RSC Adv.* 8(2018)30986-30993.

[54] Y. Zare, K. Y. Rhee, "Dependence of Z Parameter for Tensile Strength of Multi-Layered Interphase in Polymer Nanocomposites to Material and Interphase Properties" *Nanoscale Res. Lett. (2017)* 12:42.